



## **Numerical Simulation of Whistles Using Lattice Boltzmann Methods**

Y. Shi<sup>a</sup>, A. Da Silva<sup>b</sup> and G. Scavone<sup>a</sup>

<sup>a</sup>Computational Acoustic Modeling Laboratory (CAML), Centre for Interdisciplinary Research in Music Media and Technology (CIRMMT), McGill University, 555 Rue Sherbrooke Ouest, Montreal, QC, Canada H3A 1E3

<sup>b</sup>Federal Uni. of Santa Catarina, Campus Universitário Reitor João, David Ferreira Lima, Trindade, 88040-900 Florianópolis, Brazil  
yong.shi2@mail.mcgill.ca

### Abstract

The aeroacoustics of a whistle have been investigated using a physical model based on the lattice Boltzmann methods (LBM) in two dimensions. The geometric data has been measured directly from a real whistle and converted to a straightforward curved boundary in the LBM scheme with a relatively high resolution. A multiple relaxation time (MRT) technique has been employed to maintain the numerical stability and consequently a more realistic low viscosity can be used in the simulation. An absorbing boundary condition (ABC) has been used on the four outside boundaries to simulate an open space. The exciting jet is generated from a rectangular jet channel attached to the mouth of the whistle, where the velocity boundary is implemented by an ABC scheme with a non-zero target velocity. The computation has been carried out efficiently using parallel computing based on GPU devices with a speedup factor of about 20. The vortex motion in the regions around the labium that is essential for sound production has been qualitatively observed in the simulations. These images are similar to those reported in previous works based on experimental visualization and numerical simulations. Further, the sound spectrum and frequency shift phenomenon under various blowing speeds has been presented.

## 1 Introduction

The sound production of aerodynamic whistles and air-reed instruments, or the phenomenon of flow-excited acoustic resonance in general, is subject to the interaction of two closely integrated systems: the aerodynamic generator, which includes an air jet impinging on a sharp edge (the labium) acting as an acoustic dipole, and the ancillary structure functioning as an acoustic resonator.

Depending on the sound generating mechanisms, Chanaud [1] categorized aerodynamic whistles into three classes. Class I whistles only consist of purely hydrodynamic oscillations such as aeolian tones. Class II whistles involve direct acoustic feedback but without any ancillary structures. Examples of this type of whistle include edge tones, hole tones, ring tones and human whistling, etc. Class III whistles are those featured by a resonant or reflecting structure controlling the frequency of the tone.

The musical instruments of Class III include the ocarina, Chinese Xun, Japanese tsuchibue, etc., and the flute-like instruments, such as flute, organ pipe, recorder, etc. The ocarina-type instruments are distinguished by a Helmholtz resonator. On the other hand, the resonator of a flute-like instrument consists of a pipe-like air column. We consider the sport whistle as a special ocarina-type instruments characterized by a Helmholtz resonator excited by the edge tone.

The edge tone phenomenon, produced by blowing a jet of air that impinges on a sharp edge, has been investigated by a number of authors but its mechanics are still not completely understood. Since some decades ago, the theory and empirical formulas for edge tones have been presented by a number of authors ([2], [3], [4], [5], [6], [7]). Brown [2] might be the pioneer who experimentally investigated the edge tone. In his apparatus, both the velocity of the air exiting a brass slit and the distance of wedge-to-orifice can be adjusted. Using a setting of constant jet velocity, he found the threshold of distances for the onset and extinction of an edge tone. Then using a setting of constant distance, he demonstrated four stable stages of edge tone related to different velocities. The dependence of the frequency  $f$  of the edge tone on the distance  $h$  and the jet velocity  $U$  for a specific slit width of 1.0 mm is described by an empirical formula:

$$f = 0.466k(U - 40.0)(1/h - 0.07) \quad (1)$$

where  $k = 1, 2, 3, 3.8$  and  $5.4$  are coefficients related to the four different stages corresponding to the fundamental frequency and other overtones. In the same stage, the

frequency of oscillation is in proportion to the jet velocity  $U$ , but it jumps to another stage hysteretically if  $U$  exceeds a threshold value. In another paper [8], Brown provided valuable discussion regarding the interaction between edge tones and pipe tones.

The objective of this paper is to investigate the aeroacoustic behavior of a whistle using numerical simulations. This paper is structured as follows: In Section 2, we discuss the previous studies of numerical simulations of musical instruments. Section 3 describes the numerical technique used in this study. In Section 4, we first present the visualization of the jet formation and oscillation obtained in the simulation of a whistle. Then we show the frequency change phenomenon as the jet speed increases. Section 5 provides a discussion of the results and suggestions for further investigations.

## 2 Previous Numerical Modeling

In the last two decades, there has been growing interest in the use of computational fluid dynamic (CFD) tools or computational aeroacoustic (CAA) techniques based on the Navier-Stokes equations to investigate the aeroacoustic behaviors of edge tones and the more complicated phenomenon related to acoustical feedback from an ancillary resonator. However, the direct numerical simulation (DNS) of aero-acoustic problem is still expensive and limited to simple geometries and short time scales (typically 10 to 20 ms), due to the huge consumption of computing resources.

Dougherty et al. [9] numerically replicated Brown's experiments of edge tone including all four stages by using a compressible full Navier-Stokes flow solver based on a finite-volume scheme and obtained excellent agreement on frequency results compared with Brown's data. The direct simulation of flute-like instruments can be found in more recent literature by Obikane et al. and Giordano [10], [11], [12], [13], [14]. Giordano simulated a recorder using a two-dimensional and then a three-dimensional Navier-Stokes solver based on a finite difference scheme and presented both qualitative results concerning dynamics of the density and air jet, and quantitative results for the sound spectrum and its dependence on blowing speed. On the other hand, the numerical simulation of ocarina-type instruments is less commonly found in literature. Kobayashi et al. [15] reproduced the sound vibration of an ocarina and investigated the relationship between the oscillation frequencies and the blowing speed using compressible large-eddy simulations (LES). Miyamoto et al. [16] simulated a

recorder-like instrument using the LES method and showed interesting results including spatial distributions of air density, flow velocity, vorticity and Lighthill's aeroacoustic source. They also compared the changes of frequencies with jet velocity to both edge tone and resonance frequencies of the pipe. Liu [17] simulated a pea-less whistle using a hybrid CFD scheme and compared the frequencies with the experimentally measured results. But as Kobayashi pointed out [15], the hybrid model consisting of separate stages of fluid mechanics and sound propagation is not well suited for simulating a Helmholtz resonance subjected to the elastic property of air.

Compared to conventional continuum-based DNS techniques, the lattice Boltzmann method (LBM) seems a promising alternative. The LBM directly simulates the propagation and collision involving the space-time evolution of the fluid particles in a mesoscopic level in a single step. The numerical solution of the Boltzmann equation is relatively simple compared to the Navier-Stokes equations, and can be easily implemented in a parallel computation scheme. This is advantageous for simulating problems involving complicated boundary conditions.

The LBM modeling of flue instruments was pioneered by Skordo's work on recorders and organ pipes [18]. He simulated the interaction between fluid flow and the acoustic waves within the instruments at different blowing speeds based on a two-dimensional model. Kühnelt [19], [20], [21], [22], simulated several flute-like instruments including organ pipe and square flue pipe using three-dimensional LB models and obtained interesting results including the visualization of jet formation and vortex motion, the time history of fluctuating density and the steady state spectra at different jet speeds. Unfortunately, due to the restriction of computer resources, Kühnelt's models are based on rather simplified geometries with a large lattice spacing (in the range from  $\delta x = 0.175$  to  $0.3$  mm). Also, he had to increase the viscosity by 10 times higher than air to maintain the numerical stability, and consequently increase the jet speed by the same factor to get an identical Reynolds number.

In this study, we carried out the simulation of pea-less sport whistles using the two-dimensional LBM. On one hand, the relatively simple implementation of boundary conditions of the LBM allows us to handle the complicated curved boundary measured from a real whistle. On the other hand, the efficiency of our computation is greatly improved by using a parallel computing technique based on a low-cost Nvidia GPU graphic card installed on a personal computer. We used the multiple relaxation time (MRT) scheme to maintain the numerical stability and consequently we were able to use a more realistic, lower viscosity appropriate for air in our simulations. This is essential for modeling a whistle since the single relaxation time (SRT) scheme is not numerically stable for conditions involving the low viscosity of the air and the relatively high jet speeds found in normal playing condition of a whistle. However, we should keep in mind that the LBM is only compressible in the Mach number lower than about 0.15. In our simulations, therefore, the blowing speeds are restricted to relatively low values.

### 3 Numerical Procedure

Figure 1 shows pea-less whistles of different size and color which can be found at many convenient stores. The structure of a whistle consists of a narrow flue channel and a cavity resembling a Helmholtz resonator. The cross-sectional area of the opening at the end of the flue channel, or the flue exit, is smaller than the inlet, such that the jet flow is accelerated before it leaves the flue exit. It is known that the sound of a whistle combines both edge tone and Helmholtz resonance sounds [1]. As the jet impinges upon the edge of aperture of the cavity, the force exerted by the edge on the flow acts as an acoustic dipole which creates sound oscillations. Part of the sound field propagates back towards the orifice where the flow is more sensitive to disturbances.

In this way, the oscillation is reinforced and maintained and the feedback cycle is completed. This is how the edge tone is established. Meanwhile, the edge tone excites the Helmholtz resonator such that sound energy is reinforced for the preferred resonance frequency.



Figure 1: The whistles.

The purpose of the LBM scheme presented here is to reproduce the sound oscillation of a whistle in the presence of a low Mach flow. General descriptions of the lattice Boltzmann method can be found in books by Succi [23], Gladrow [24] and Guo and Shu [25].

The LBM scheme is described by thin walls resembling the cross section of a whistle immersed in a fluid domain surrounded by open boundaries. The fluid domain is represented by a rectangular D2Q9 structure [26]. The left, right, top and bottom boundaries of the radiation domain are implemented by absorbing boundary conditions prescribed with a zero velocity, as proposed by Kam et al. [27].

We generated 2D thin curved boundaries based on the geometry profile measured from the clear whistle (Whistle I) and the red whistle (Whistle II) shown in Fig. 1. The curved boundaries were then imported into the 2D LB model by a custom Python script, as shown in Fig. 2. The height  $H$  and the width  $W$  of the open mouth of the resonance cavity of the two whistles are given in Table 1. Whistle I features a smaller ratio of  $W/H$  and a smooth wall inside the wind channel. The walls are treated by a simple bounce-back scheme [23], which creates a no-slip condition at the wall and simulates a viscous boundary layer.

The size of the LB model representing the two whistle is given in Table 2, where  $nX$  and  $nY$  are the number of lattice cells along the x- and y-axis, respectively. The space

	H (mm)	W(mm)
Whistle I	1.245	12.7
Whistle II	0.45	13.15

Table 1: Height and width of the two whistles

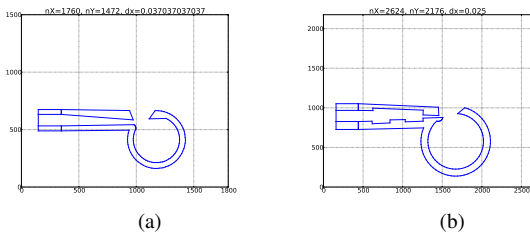


Figure 2: The B.C. of the whistles. (a) Whistle I (b) Whistle II

resolution  $dx$  representing the unit length of one lattice cell is decided by both the available computing resources and the smallest geometrical length of the boundary, which is the height  $H$  measured at the exit of the flue channel for our specific case. The number of lattice cells representing the height  $H$  is 40 for Whistle I and 18 for Whistle II, respectively, which is sufficient in consideration of both stability and accuracy, according to our previous experiences.

	nX	nY	dx (mm)
Whistle I	1760	1472	0.037
Whistle II	2624	2176	0.025

Table 2: Size of the two LB models

Skordos and Kühnelt ([18], [19], [20], [21], [22]) used unrealistic higher viscosities in their LBM scheme to maintain numerical stability. This was most likely due to the restriction of the Single Relaxation Time (SRT) scheme, which is prone to be unstable in conditions of very low viscosities. In order to improve computational stability and allow the use of a viscosity more representative of air, we chose to use the Multiple Relaxation Time (MRT) scheme [28], [25]. The MRT lattice Boltzmann equation (LBE) evolves the collision step in the velocity space and the streaming step in moment space:

$$\mathbf{f}(\mathbf{x}, t + \Delta t) = \mathbf{f}(\mathbf{x}, t) - \mathbf{M}^{-1} \mathbf{S}(\mathbf{m} - \mathbf{m}^{eq}), \quad (2)$$

where  $\mathbf{f}$  is the distribution function,  $\mathbf{M}$  is the relaxation matrix related to numerical viscosity,  $\mathbf{S} = \mathbf{M} \mathbf{M}^{-1}$  is a diagonal matrix, and  $\mathbf{m} = \mathbf{M} \mathbf{f}$  is the equilibria in the moment space. The MRT greatly improves the stability of the system at very low viscosity with a cost of an additional computation time of about 20%.

The dimensionless kinematic viscosity  $\nu$  can be calculated from the physical kinematic viscosity of air  $\nu^*$  and the space resolution  $dx$  by the relation  $\nu^* = \frac{\nu c_s^* dx}{c_s}$ , where  $c_s^*$  is the physical speed of the sound and  $c_s$  is the speed of sound in lattice unit. The undisturbed fluid density was set as  $\rho_0 = 1.0 \text{ kg/m}^3$  for convenience.

The source flow is implemented by a source buffer attached at the left end of the flue channel using absorbing boundary conditions with a non-zero target velocity prescribed by the source signal. The jet speed is measured at the center of the flue exit.

The time histories of fluid density are probed above the open mouth at a sampling rate of 80 kHz, where the coordinates of the probing point is ( $x=1000$ ,  $y=800$ ) for Whistle I and ( $x=1400$ ,  $y=1100$ ) for Whistle II. A zero-phase DC-blocking filter must be used in the post-processing to remove the fluctuation caused by the fluid flow.

The LB model is implemented by a custom parallel computing code written in Pycuda [29], and runs on a desktop PC equipped with a Nvidia GeForce GTX 670 graphics card. A simple test using a lattice of 1000 by 1000 cells running on the GPU indicated a speed-up factor of approximately 20 (0.053 vs. 1.06 seconds per iteration) compared to the same model running on the CPU in serial mode.

## 4 Results

### 4.1 Jet Formation and Oscillation

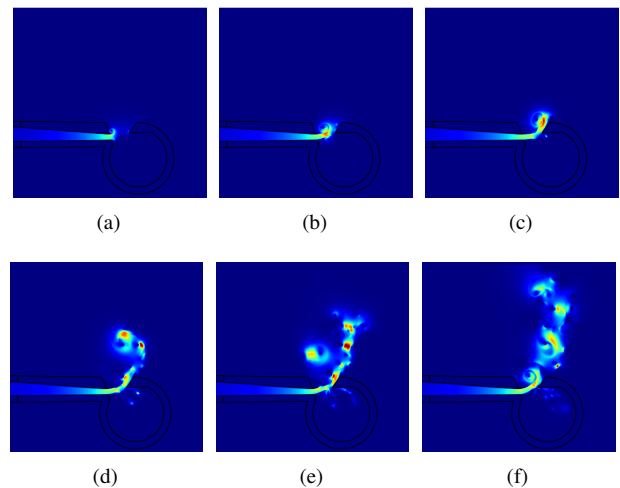


Figure 3: The formation of the jet during start-up. The colors represent the absolute value of velocity ( $\sqrt{u_x^2 + u_y^2}$ ). The red color corresponds to the highest speed and the dark blue to the lowest speed. For the simulation the jet speed at the center of the flue exit is  $U_{jet} = 30 \text{ m/s}$ .

Figure 3 shows how the jet is formed at the start-up stage. The formation of the first vortex is demonstrated in Fig. 3(a) - 3(c). The vortex shedding above and below the flue exit are also clearly visible, as shown in Fig. 3(c) - 3(f).

Figure 4 shows motion of the jet around the labium during the course of one cycle for Whistle I at  $U_{jet} = 30 \text{ m/s}$ . The air jet oscillates mainly above the labium. This behavior is qualitatively similar to that found in a 2D DNS of a recorder by Giordano [13], but different from that observed in a 3D DNS carried out by the same author [14]. According to Miyamoto [30], this phenomenon is due to differences in energy dissipation and vortex motion in two and three dimensions.

### 4.2 Sound Oscillation

The time histories of the acoustic density in numerical units for four different jet speeds ( $U_{jet} = 10, 20, 30$  and  $40 \text{ m/s}$ ) are shown in Fig. 5. The amplitude of the signal at the start-up stage is almost in linear proportion to the jet speed, as

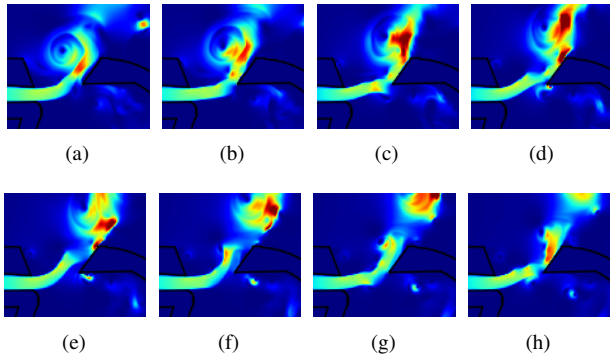


Figure 4: Images of the air speed near the flue channel exit and labium of Whistle I during one cycle. The colors represent the absolute value of velocity ( $\sqrt{u_x^2 + u_y^2}$ ). The red color corresponds to the highest speed and the dark blue to the lowest speed. For the simulation the jet speed at the center of the flue channel is  $U_{jet} = 30$  m/s.

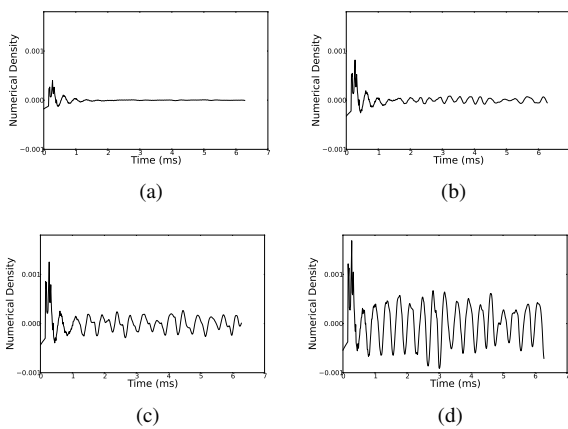


Figure 5: Numerical density of whistle I with various jet speed. Jet speed: (a),  $U_{jet} = 10$  m/s. (b),  $U_{jet} = 20$  m/s. (c),  $U_{jet} = 30$  m/s. (d),  $U_{jet} = 40$  m/s.

we will find later. The oscillation is not visible for  $U_{jet} = 10$ , though it is visible for the other three higher jet speeds.

The normalized spectrum of the simulation for three different jet speeds are depicted in Fig. 6. For  $U_{jet} = 20$  m/s, there is almost no harmonics found in the result, suggesting the typical behavior of a Helmholtz resonance. For  $U_{jet} = 30$  and 40 m/s, harmonics emerge in the results. The simulation results show a relatively high level of noise compared to the peak frequency, which is probably due to the rather short simulation time which is insufficient for the build-up of a steady oscillation.

### 4.3 Change of Frequency and Amplitude with Jet Speed

Figure 7(a) shows the change of peak frequency with increase of jet speed  $U_{jet}$  in the simulation of Whistle I. The edge tone frequencies of the four stages given by Brown's empirical equation (Eq. 1) are also depicted (fb1, fb2, fb3 and fb4). No overtone is observed, which is typical for Helmholtz-type resonators. In the range of  $13 \leq U_{jet} \leq 18$ , the simulation results are close to the curve of fb4, the fourth stage of Brown's edge tone, but this might be only a coincidence, because the oscillation is not stable for

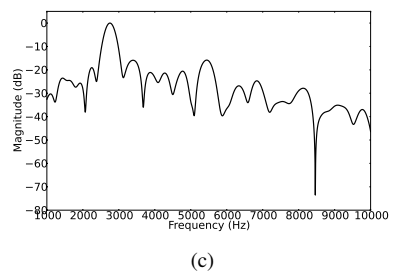
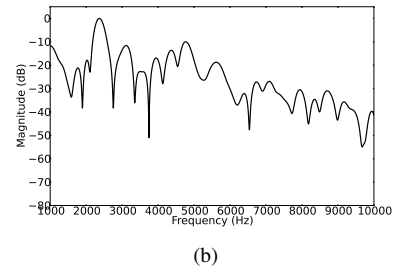
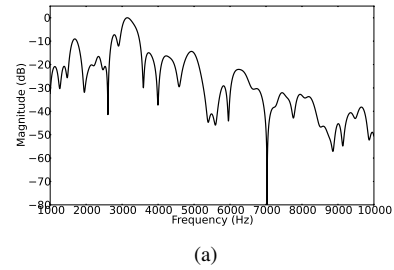


Figure 6: Normalized spectrum of whistle I with various jet speeds: (a),  $U_{jet} = 20$  m/s. (b),  $U_{jet} = 30$  m/s. (c),  $U_{jet} = 40$  m/s.

low jet speeds. A transition is observed in the range of  $20 < U_{jet} < 25$ . For jet speeds beyond 25, the simulation results are very close to the edge tone curve.

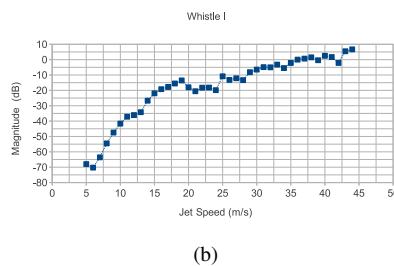
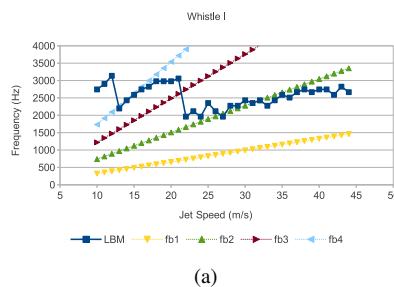


Figure 7: Peak frequency and normalized magnitude of whistle I for various jet speeds. 7(a): peak frequency and frequency of edge tone (fb1, fb2, fb3 and fb4, see Eq. 1), (b) normalized magnitude.

The same comparison of the change of peak frequency with increase of jet speed is made for Whistle II, as depicted

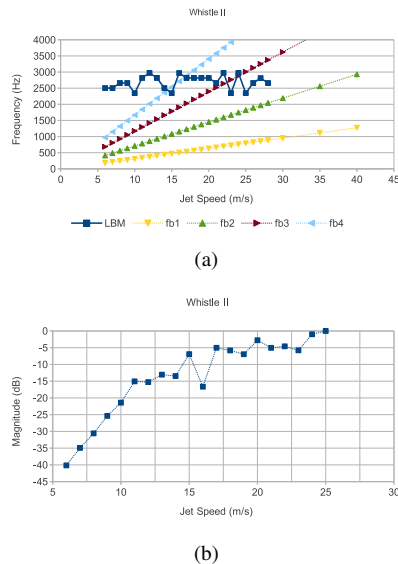


Figure 8: Peak frequency and normalized magnitude of whistle II for various jet speeds. (a): peak frequency and frequencies of edge tone (fb1, fb2, fb3 and fb4, see Eq. 1), (b) normalized magnitude.

in Fig. 8(a). We notice fluctuations of the frequencies for jet speeds higher than 20 m/s, which is not surprising because the simulation is terminated before the steady acoustic oscillation can be developed.

The magnitudes of the peak frequency of simulation are depicted in Fig. 7(b) for Whistle I and Fig. 8(b) for Whistle II. The curve is normalized to 0 dB for jet speed at  $U_{jet} = 36$  for Whistle I and  $U_{jet} = 25$  for Whistle II. Overall, the amplitude increases almost linearly for jet speeds less than 10 m/s. We can observe some fluctuations and slight drops in the range of  $20 < U_{jet} < 25$  for Whistle I and  $15 < U_{jet} < 20$  and  $20 < U_{jet} < 25$  for Whistle II.

The results reported above are in partial agreement with measured data known to the authors but not available for publication at this time. In particular, the peak frequencies in the spectrum of the simulation are close to those of the measured results, and similarities have been found in the change of frequency with the increasing jet speed. The measured results display a general increase of oscillation frequency with jet speed, except for a transition zone found in the mid-range of jet speeds ( $20 < U_{jet} < 25$ ). The frequency curves of both simulations and measured results of Whistle I are close to the edge tone curve for higher jet speeds ( $U_{jet} \geq 25$ ). On the other hand, the measured results show a dip in the magnitude of the peak frequencies in the mid-range of jet speeds (in the transition zone) that was not observed in the LBM results.

## 5 Conclusions

We have presented results from a two dimensional LBM simulation of whistles, including 1) the qualitative visualization of the jet formation and vortex shedding, and 2) the quantitative results of the spectrum and the change of peak frequencies for various jet speeds. We are able to use a low viscosity thanks to the MRT technique. Also, the simulation speed is greatly improved by the parallel GPU computing, which makes it feasible for more simulations,

longer simulation time, larger fluid domain and higher space resolutions.

However, the actual simulation time is still restricted by some factors. The fluid vorticity is not well absorbed by the absorbing boundary conditions, which results in spurious reflections from the open boundaries after a certain amount of iterations. Even with the help of MRT, the numerical stability for conditions of relatively high jet speeds is not well maintained after a certain amount of iterations. The Mach number in LBM is limited to about 0.15, or even lower for low viscosity cases, so it is not capable of handling all possible jet speeds found in a typical whistle. Nonetheless, for flute-like instruments with relatively low jet speeds, such as the recorder and organ pipes, the LBM can be a good simulation tool.

## Acknowledgments

The authors wish to acknowledge funding from the Fonds québécois de la recherche sur la nature et les technologies (FQRNT), the Natural Sciences and Engineering Research Council of Canada (NSERC), and the Centre for Interdisciplinary Research in Music Media and Technology.

## References

- [1] R. C. Chanaud, "Aerodynamic whistles," *Scientific American*, vol. 222, pp. 40–47, 1970.
- [2] G. B. Brown, "The vortex motion causing edge tones," *Proceedings of the Physical Society*, vol. 49, no. 5, p. 493, 1937.
- [3] G. B. Brown, "The mechanism of edge-tone production," *Proceedings of the Physical Society*, vol. 49, no. 5, p. 508, 1937.
- [4] N. Curle, "The mechanics of edge-tones," *Proceedings of the Royal Society of London. Series A. Mathematical and Physical Sciences*, vol. 216, no. 1126, pp. 412–424, 1953.
- [5] A. Powell, "On the edgetone," *The Journal of the Acoustical Society of America*, vol. 33, no. 4, pp. 395–409, 1961.
- [6] J. W. Coltman, "Sounding mechanism of the flute and organ pipe," *The Journal of the Acoustical Society of America*, vol. 44, no. 4, pp. 983–992, 1968.
- [7] J. W. Coltman, "Jet drive mechanisms in edge tones and organ pipes," *The Journal of the Acoustical Society of America*, vol. 60, no. 3, pp. 725–733, 1976.
- [8] G. B. Brown, "Organ pipes and edge tones," *Nature*, vol. 141, pp. 11–13, 1938.
- [9] N. Dougherty, B. Liu, and J. O'Farrell, "Numerical simulation of the edge tone phenomenon," National Aeronautics and Space Administration, Office of Management, Scientific and Technical Information Program, Tech. Rep., 1994.

- [10] Y. Obikane and K. Kuwahara, "Direct simulation for acoustic near fields using the compressible navier-stokes equation," in *Computational Fluid Dynamics 2008*. Springer, 2009, pp. 85–91.
- [11] Y. Obikane, "Direct simulation on a fipple flute using the compressible navier-stokes equation," *World Acad. Sci., Eng. Technol.*, vol. 4, pp. 794–798, 2009.
- [12] Y. Obikane, "Computational aeroacoustics on a small flute using a direct simulation," in *Computational Fluid Dynamics 2010*. Springer, 2011, pp. 435–441.
- [13] N. Giordano, "Direct numerical simulation of a recorder," *The Journal of the Acoustical Society of America*, vol. 133, no. 2, pp. 1111–1118, 2013.
- [14] N. Giordano, "Simulation studies of a recorder in three dimensions," *The Journal of the Acoustical Society of America*, vol. 135, no. 2, pp. 906–916, 2014.
- [15] T. Kobayashi, T. Takami, M. Miyamoto, K. Takahashi, A. Nishida, and M. Aoyagi, "3d calculation with compressible les for sound vibration of ocarina," *arXiv preprint arXiv:0911.3567*, 2009.
- [16] M. Miyamoto, Y. Ito, K. Takahashi, T. Takami, T. Kobayashi, A. Nishida, and M. Aoyagi, "Applicability of compressible les to reproduction of sound vibration of an air-reed instrument," in *Proceedings of the International Symposium on Musical Acoustics, Sydney and Katoomba, Australia*, 2010.
- [17] J. Liu, "Simulation of whistle noise using computational fluid dynamics and acoustic finite element simulation," mastersthesi, University of Kentucky, Lexington, Kentucky, 2012.
- [18] P. Skordos, "Modeling flue pipes: subsonic flow, lattice boltzmann, and parallel distributed computers," Ph.D. dissertation, Massachusetts Institute of Technology, 1995.
- [19] H. Kühnelt, "Simulating the mechanism of sound generation in flutes using the lattice boltzmann method," in *Proceedings of the Stockholm Music Acoustics Conference*, 2003.
- [20] H. Kühnelt, "Simulating the sound generation in flutes and flue pipes with the lattice-boltzmann-method," in *Proc. Int. Symp. Musical Acoustics, Nara, Japan, 2004*, 2004.
- [21] H. Kühnelt, "Simulation and analysis of the flow-acoustic interactions in the mouth of flute-like instruments," in *Forum Acusticum (European Conference on Acoustics), Budapest*, 2005, pp. 1–6.
- [22] H. Kühnelt, "Vortex sound in recorder- and flute-like instruments: Numerical simulation and analysis," in *Proc. Int. Symp. Music. Acoust.*, 2007.
- [23] S. Succi, *The lattice Boltzmann equation for fluid dynamics and beyond*. Oxford University Press, 2001.
- [24] D. A. Wolf-Gladrow, *Lattice Gas Cellular Automata and Lattice Boltzmann Models: An Introduction. Lecture Notes in Mathematics*. Springer, Berlin / Heidelberg, 2004.
- [25] Z. Guo and C. Shu, *Lattice Boltzmann Method and Its Applications in Engineering*. World Scientific Publishing, 2013.
- [26] Y. Qian, D. d'Humieres, and P. Lallemand, "Lattice BGK models for Navier-Stokes equation," *Europhysics Letters*, vol. 17, no. 6, pp. 479–484, 1992.
- [27] E. Kam, R. So, and R. Leung, "Non-reflecting boundary conditions for one-step LBM simulation of aeroacoustics," in *27th AIAA Aeroacoustics Conference, 8-10 May 2006, Cambridge, Massachusetts*, 2006.
- [28] D. d'Humieres, "Generalized lattice-boltzmann equations," *Rarefied gas dynamics- Theory and simulations*, pp. 450–458, 1994.
- [29] A. Klöckner, N. Pinto, Y. Lee, B. Catanzaro, P. Ivanov, A. Fasih, A. Sarma, D. Nanongkai, G. Pandurangan, P. Tetali *et al.*, "Pycuda: Gpu run-time code generation for high-performance computing," *Arxiv preprint arXiv*, vol. 911, 2009.
- [30] M. Miyamoto, Y. Ito, T. Iwasaki, T. Akamura, K. Takahashi, T. Takami, T. Kobayashi, A. Nishida, and M. Aoyagi, "Numerical study on acoustic oscillations of 2d and 3d flue organ pipe like instruments with compressible les," *Acta Acustica united with Acustica*, vol. 99, no. 1, pp. 154–171, 2013.